Free-carrier dynamics and band tails in Cu$_2$ZnSn(S$_x$Se$_{1-x}$)$_4$: Evaluation of factors determining solar cell efficiency

Le Quang Phuong,[1,2] Makoto Okano,[1] Genki Yamashita,[3] Masaya Nagai,[3] Masaaki Ashida,[3] Akira Nagaoka,[4,5] Kenji Yoshino,[5] and Yoshihiko Kanemitsu[1,2,*]

[1]*Institute for Chemical Research, Kyoto University, Uji, Kyoto 611-0011, Japan*
[2]*Japan Science and Technology Agency, CREST, Uji, Kyoto 611-0011, Japan*
[3]*Graduate School of Engineering Science, Osaka University, Osaka 560–8531, Japan*
[4]*Department of Materials Science and Engineering, Kyoto University, Kyoto 606–8501, Japan*
[5]*Department of Applied Physics and Electronic Engineering, University of Miyazaki, Miyazaki 889–2192, Japan*

We investigated the composition-dependent photocarrier dynamics in Cu$_2$ZnSn(S$_x$Se$_{1-x}$)$_4$ (CZTSSe) single crystals using various types of steady-state and time-resolved optical spectroscopy. Photoluminescence spectroscopy shows that the band-tail states formed below the band edge decrease monotonically with increasing Se content. THz time-resolved spectroscopy clarifies that an increase in the Se content leads to a shorter lifetime of the free photocarriers. A trade-off between the composition-dependent band-tail density and the free-carrier lifetime occurs in CZTSSe single crystals. Our experimental results provide insights into the physics behind the low and composition-dependent conversion efficiency of CZTSSe-based solar cells.

PACS number(s): 78.55.Hx, 88.40.jn, 78.47.D−, 78.47.jg

I. INTRODUCTION

Recently, the efficiency of converting solar energy to electrical energy has been increasingly improved in many types of solar cells [1]. The multinary semiconductor Cu$_2$ZnSn(S$_x$Se$_{1-x}$)$_4$ (CZTSSe) has attracted extensive attention as an emerging light absorber for next-generation, low-cost, thin-film solar cells due to its excellent characteristics for solar energy conversion and earth-abundant-element composition [2,3]. The band-gap energy of CZTSSe can be tuned to optimize the absorption of solar light through adjusting the relative composition of the anions S and Se [2,4]. It has been empirically established that a CZTSSe absorber with a Se-rich composition usually leads to a better photovoltaic performance of CZTSSe-based solar cells [5–7]. Presently, solar cells with maximum power conversion efficiencies (PCEs) of 8.4% [5] and 11.6% [6] can be produced based on pure-sulfide CZTS and pure-selenide CZTSe thin-film absorbers, which have band-gap energies of ~1.5 and ~1.0 eV, respectively. Meanwhile, using an anion-mixture (Se-rich) CZTSSe absorber with a band-gap energy of 1.13 eV resulted in a state-of-the-art 12.6% PCE for CZTSSe-based solar cells [7]. On the other hand, solar cells with PCEs exceeding 20% have been already achieved using a CuIn$_{1-x}$Ga$_x$Se (CIGS) absorber with a band-gap energy of 1.14 eV, almost equal to that of the absorber in the best CZTSSe-based solar cells [7,8]. It is plausible that the band-gap energy of the absorber is not the only reason causing the low and composition-dependent PCEs of CZTSSe-based solar cells. Therefore, it is essential to understand the other physical mechanisms that determine and limit the PCE of CZTSSe-based solar cells in order to appropriately direct further efforts to improve their performance. In addition, a combination of various optical techniques is fruitful for a thorough understanding of the optoelectronic properties of emerging solar-cell materials [9–11].

In this paper, we investigated the composition dependence of photocarrier dynamics in CZTSSe single crystals using a combination of various types of steady-state and time-resolved optical spectroscopy. In addition to the band-gap energy, the band tails, which exist below the band edge and cause a reduction in the PCE of solar cells, were found to decrease monotonically with increasing Se content. Surprisingly, an increase in the Se concentration leads to a shorter lifetime of the photocarriers in CZTSSe. Our experimental results reveal explicitly the physics behind the observed composition dependence of the PCE of CZTSSe-based solar cells and explain why it is much smaller than that of CIGS-based ones.

II. EXPERIMENT

CZTSSe single crystals were fabricated using the traveling heater method [12]. The anion composition was determined by electron probe microanalysis. For photoluminescene excitation (PLE) measurements, a broadband white-light picosecond laser equipped with a band-pass transmission filter was used as the photoexcitation source. For the steady-state and time-resolved photoluminescence (PL) measurements, a pulse emitted from an optical parametric amplifier pumped by an Yb:KGW regenerative amplified laser with a pulse duration of ~300 fs and a repetition rate 50–200 kHz was utilized to excite the samples. The PL signal was collected using a backward configuration and directed to 30-cm monochromators (with a grating 150 grooves/mm) equipped with a liquid-nitrogen-cooled InGaAs photodiode array or a Si charged-coupled device (CCD). The spectral responses of all the PL measurements were calibrated using a standard lamp.

In optical pump–white-light probe transient reflectivity (TR) measurements, a pulse from the same excitation source as that used in the PL measurements was chopped with a frequency of 130 Hz (for the integration of signals) and

---

*Corresponding author: kanemitu@scl.kyoto-u.ac.jp

irradiated onto the sample for pump photoexcitation. The excitation photon energy was tuned from 1.69 to 2.75 eV for different samples. A part of the fundamental pulse from the Yb:KGW regenerative amplified laser was focused on a sapphire crystal to generate a white-light probe pulse. The reflection of the probe pulse from the excitation spot was collected through a monochromator. The TR signal was obtained by comparing the reflectivity of probe pulses with and without pump pulse excitation.

Optical pump–THz probe TR (THz-TR) measurements were performed using a Ti:sapphire regenerative amplified laser (1-kHz repetition rate and 35-fs pulse duration). Wavelength-tunable excitation pump pulses emitted from an optical parametric amplifier were chopped with a frequency of 250 Hz, and the collimated excitation beam was then guided to the samples, which were attached to a metal plate with a 2-mm-diameter hole. A THz-probe pulse with a center frequency of 1 THz generated from two-color pumped air plasma was directed to the excitation spot with an incident angle of $30°$. The electric-field profile of the reflected THz pulse was detected using the electro-optic sampling method utilizing a 1-mm-thick ZnTe crystal. The detectable frequency ranged from 0.5 to 2.5 THz. All optical measurements were conducted at room temperature.

III. RESULTS AND DISCUSSION

Figure 1(a) shows representative normalized PL (solid red) and PLE (solid blue) spectra of CZTSSe samples with different S concentrations ($x = 0$, 0.5, 0.8, and 1.0) measured under weak photoexcitation. A typical PLE spectrum of CZTSSe

samples shows a significant tail in the low-energy region, a broad peak structure, whose energetic location depends obviously on the anion composition, and a reduction in the high-energy region. Under high-energy photoexcitation, photocarriers are generated near the surface region of the CZTSSe samples, where a larger number of nonradiative recombination centers exist [13–15]. The high-energy-side decrease in the PLE spectrum thus is due to an enhancement of nonradiative recombination occurring near the surface region [13–15]. Based on various experimental techniques including PLE, photocurrent, and TR measurements, we have previously shown that the band-gap energy of the pure-sulfide CZTSSe sample ($x = 1.0$) could be determined approximately around the PLE peak energy [14]. In this paper, we use a fitting procedure for the low-energy-side tail of the PLE spectrum as a universal tool to evaluate more quantitatively and accurately the band-gap energies of CZTSSe samples with different compositions.

Owing to the existence of a considerable number of ionized defects in the multinary compound CZTSSe [16], large electrostatic potential fluctuations occur and modify the near-band-edge structure, leading to the formation of high-density band tails below the band edge [14,15,17–21]. The exponential tail detected in the low-energy side of the PLE spectrum reflects the light absorption of the below-band-edge tails, this has been calculated theoretically to be only a function of the band-gap energy E_g and the average amplitude of the electrostatic potential fluctuations γ [19,22]. The amplitude of γ depends monotonically on the density of charged defects and can be evaluated from the charged defect density, dielectric constant, and effective masses of electrons and holes. By using
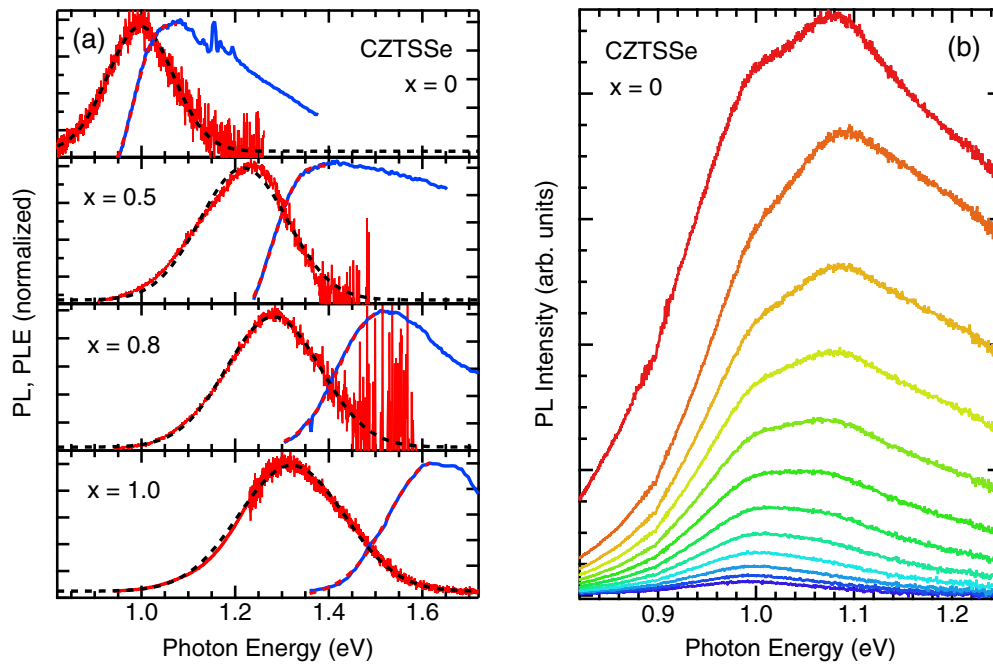

FIG. 1. (Color online) (a) Normalized PL (solid red curves: obtained under weak 1.6-eV photoexcitation for the samples with $x = 0$, 0.5, and 0.8 and under weak 1.65-eV photoexcitation for the sample with $x = 1$) and PLE (solid blue curves) spectra of CZTSSe with different S content ($x = 0$, 0.5, 0.8, and 1.0). The PL spectrum of the CZTS ($x = 1.0$) is composed of two PL spectra measured with an InGaAs photodiode array (for the low-energy region) and a Si CCD (for the high-energy region). The dashed black and red curves are fitting curves of PL and PLE spectra, respectively. (b) PL spectra of the pure-selenide CZTSSe sample ($x = 0$) under different fluences (darkest blue curve: 0.06 mJ cm^{-2}; red curve: ~5 mJ cm^{-2}) of the 1.6-eV photoexcitation.

the below-band-edge absorption coefficient α [19,22,23],

$$\alpha \propto \exp\left(-\frac{2}{5\sqrt{\pi}}\left(\frac{E_g - \hbar\omega}{\frac{\gamma}{2}}\right)^{\frac{5}{4}}\right), \qquad (1)$$

the low-energy tails of the PLE spectra can be well reproduced, as shown by the dashed red curves in Fig. 1(a). For the pure-selenide CZTSSe sample ($x = 0$), a band-gap energy E_g of 1.08 ± 0.03 eV was estimated from the fitting procedure. Similar band-gap energies of pure-selenide CZTSSe polycrystalline thin films were reported in previous papers [4,24]. In addition, it is important to note that the obtained band-gap energy of pure-sulfide CZTSSe sample ($x = 1$) $E_g = 1.61 \pm 0.03$ eV is consistent with our previous estimation using other experimental methods [14].

Figure 1(b) shows the PL spectra of pure-selenide CZTSSe ($x = 0$) obtained under difference fluences of the 1.6-eV photoexcitation. A single, broad PL band with peak energy of $\sim$0.99 eV appears in the low-energy side of the PLE spectrum under weak excitation fluences. An additional high-energy PL band peaking at $\sim$1.08 eV emerges and dominates under strong excitation fluences. The low-energy 0.99-eV PL band originates from the radiative recombination of photocarriers localized at the high-density band tails and deep defects below the band edge of CZTSSe [14,15,20]. Under extremely strong photoexcitation fluences, the band-to-band recombination usually arises at the high-energy side in the PL spectrum and peaking around the band-gap energy. The observed high-energy PL band of the pure-selenide CZTSSe sample, thus, is likely to originate from the band-to-band recombination. The noticeable broad PL signal above the peak energy probably relates to the complicated band structures of CZTSSe material [25], including the other valence bands and large structural inhomogeneities. The consistency between the PLE and highly excited PL spectra of the pure-selenide CZTSSe sample strongly support that the obtained values of E_g and γ of CZTSSe samples using the above fitting procedure for the low-energy tails of the PLE spectra are reliable. Here, note that the high-energy PL band was clearly observed for pure-selenide CZTSSe samples ($x = 0$) but not for the other studied samples with $x = 0.5$, 0.8, and 1.0, even under the strongest photoexcitation fluences in our experiments. We have therefore utilized the PLE measurement as an appropriate method to investigate the composition dependence of the steady-state optical responses of photocarriers in CZTSSe, as discussed in the following.

The PL spectra shown in Fig. 1(a) were fitted using a Gaussian function to evaluate their peak energies and spectral widths. The PL peak energy, the corresponding band-gap energy E_g estimated from the PLE spectra, and the PL spectral width are then plotted as a function of the S concentration in Figs. 2(a) and 2(b). The band-gap energy E_g increases almost linearly, and the PL peak energy shows a blueshift with increasing S content; these values and composition-dependent tendencies are consistent with earlier studies [24,26,27]. The spectral width of the PL band tends to be broader as the S concentration increases. Note that the PL spectral width reflects the energy distribution of defects below the band edge that are involved in the PL emission process. Therefore, the narrowing of the PL spectral width with increasing Se content
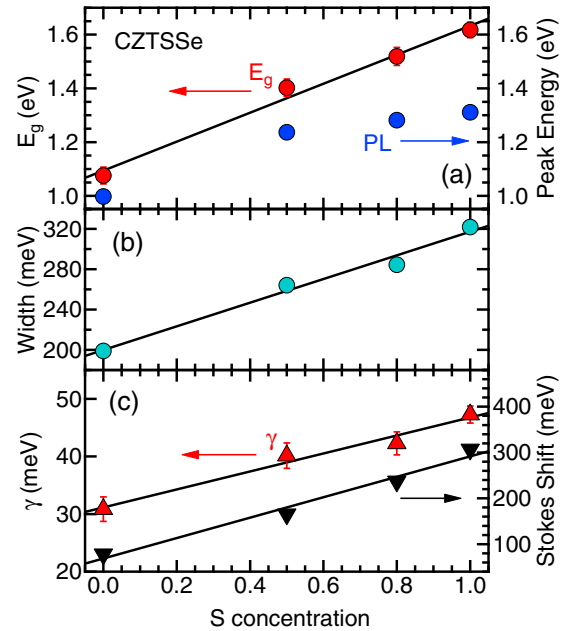

FIG. 2. (Color online) (a) The band-gap energy E_g (red circles) and the PL peak energy (blue circles), (b) the PL spectral width, and (c) the Stokes shift (black triangles) and the average amplitude of potential fluctuations γ (red triangles) as functions of the S concentration. The solid lines are guides for the eye.

indicates that some types of existing defects in the pure-sulfide CZTSSe samples ($x = 1.0$) are eliminated with the presence of Se.

The composition dependence of the Stokes shift Δ_S, which is obtained as the energy difference between the band-gap energy and the PL peak energy, and the average amplitude of potential fluctuations γ are shown in Fig. 2(c). Surprisingly, Δ_S and γ increase monotonically with increasing S content. In general, if an alloy disorder (compositional disorder) determines the PL properties of alloy samples, the maxima of the PL width, Δ_S, and γ are expected to be observed for samples with $x = 0.5$, and their minima for samples are with $x = 0$ or 1.0 [26,28]. The observed composition dependences of Δ_S and γ imply that the radiative defects become shallower, and the electrostatic potential fluctuations near the band edge tend to be smaller as the Se concentration increases. Note that γ relates to the density of charged defects according to the following equation [19,22]:

$$\gamma^5 = \left(\frac{e^2}{4\pi\epsilon_r\epsilon_0}\right)^4 \frac{N^2\hbar^2}{m_r}, \qquad (2)$$

where N is the charged defect density, ε_r is the dielectric constant, and m_r is the reduced electron/hole mass. Using this equation and the reported values of the dielectric constants and reduced electron/hole masses in CZTSSe [24,25], we found that the charged defect concentration in the pure-selenide CZTSSe sample ($x = 0$) is approximately three times smaller than that in the pure-sulfide CZTSSe ones ($x = 1.0$). Table I summarizes the composition dependences of the band-gap energy E_g, the PL peak energy, the PL spectral width, and the average depth of electrostatic potential fluctuation γ of CZTSSe samples. All these results explain why the

TABLE I. Representative values of the band-gap energy E_g, the PL peak energy, the PL spectral width, and γ of the CZTSSe samples with different S content $x = 0$, 0.5, 0.8, and 1.0.

S content	E_g(eV)	PL peak (eV)	Spectral width (meV)	γ (meV)
$x = 0$	1.08	0.99	199	31
$x = 0.5$	1.40	1.24	264	40
$x = 0.8$	1.52	1.28	284	42
$x = 1.0$	1.61	1.31	322	47

band-to-band recombination was evident for the pure-selenide CZTSSe samples ($x = 0$).

It has been theoretically predicted that if PL radiative recombination is considered as an only source for the photocarrier loss in the absorbers, the existence of high-density band tails below the band edges produces a decrease in the PCE of single-junction solar cells [29]. From this point of view, a larger γ causes a more severe reduction in the PCE. Therefore, our results provide experimental evidence supporting the empirical observation that the highly efficient CZTSSe-based solar cells so far were based on CZTSSe absorbers with Se-rich compositions [5–7]. Although γ has the smallest value for the pure-selenide samples, the band-gap energy $E_g \sim 1.08$ eV is not optimal for the absorption of solar light. Consequently, the use of an anion-mixture absorber, which has a larger band-gap energy than that of the pure-selenide absorbers, can produce solar cells with better conversion efficiencies than the pure-selenide-based solar cells [6,7].

In fact, the photocarriers in real solar cells are also dissipated through the nonradiative recombination defects in the absorbers, in addition to radiative recombination. PL and PLE spectroscopy correlate mostly to the steady-state radiative optical responses of localized photocarriers in the band tails. In contrast, time-resolved measurements provide details on the transient behavior of free photocarriers and are also sensitive to the relaxation processes to shallow and deep defects. We have therefore conducted TR and THz-TR measurements to gain a deeper understanding of the composition-dependent photocarrier relaxation and recombination dynamics in CZTSSe absorbers that essentially affect charge separation and transport in CZTSSe-based solar cells.

Figure 3(a) shows the TR decay dynamics of CZTSSe samples with $x = 0.5$ and 1.0 probed near the band-gap energies under different photoexcitation energies. The TR kinetic traces in the early-time region are well described using one fast negative decay and one rise and one slow positive decay component:

$$\frac{\Delta R}{R}(t) = A_1 \left(1 - \exp\left(-\frac{t}{\tau_{\text{rise}}}\right) \right) \exp\left(-\frac{t}{\tau_{\text{decay}}}\right) - A_2 \exp\left(-\frac{t}{\tau_{\text{decay}}^*}\right), \qquad (3)$$

where τ_{rise}, τ_{decay}, and τ_{decay}^* are the rise time and the decay time of the positive signal and the decay time of the negative signal, respectively, and A_1 and A_2 are the amplitudes of the positive and negative signals, respectively. The fast negative signal immediately after photoexcitation is caused by band-gap renormalization [30]. A rise component emerging in the photobleaching TR kinetic traces was observed. Note that the photobleaching TR decay dynamics probed around the band-gap energy demonstrates the time-dependent concentration of the photocarriers that are located near the band edge [15,30]. The rise time in the TR decay dynamics, therefore, reflects the energy relaxation of the photocarriers towards the band edge. It was also found that the rise time is independent of the excitation fluence in our experimental conditions [30]. The rise times of the photocarriers in CZTSSe with different compositions are plotted in Fig. 3(b) as functions of the excess energy, which is defined as the energy difference between the excitation and probe energies.

Obviously, the energy relaxation appears to be slower with increasing S concentration, and, in the pure-sulfide samples, it
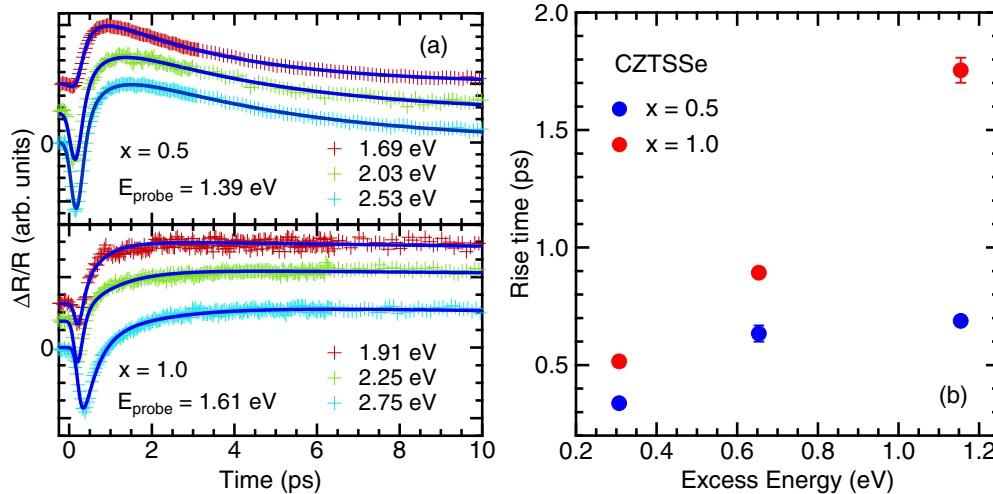

FIG. 3. (Color online) (a) TR decay dynamics probed near the band-gap energies ($\Delta R/R$) of the photocarriers in CZTSSe with $x = 0.5$ and 1.0 measured under excitations with different photon energies. The TR decay dynamics are shifted vertically for clarity. The solid curves are fitting curves. (b) The rise times of the photocarriers in CZTSSe with $x = 0.5$ (blue circles) and 1.0 (red circles) as functions of the excess energy.

is slower than that observed in conventional direct-gap semiconductors by up to a picosecond [30]. The slow energy relaxation of the photocarriers in multinary materials such as CIGS and CZTS was proposed to relate primarily to the electrostatic potential fluctuations occurring near the band edge [30,31]. The potential fluctuations form local minima above the band edge that capture repeatedly the photocarriers and slow their energy relaxation. According to this viewpoint, larger potential fluctuation, namely a larger value of γ, is expected to cause a slower energy relaxation of photocarriers. Consequently, the observed composition dependence of the energy relaxation of the photocarriers in CZTSSe could be interpreted based on the composition dependence of γ, shown in Fig. 2(c). In addition, the spatial separations of photocarriers at the local minima near the band edge lead to a suppression of carrier-carrier scattering, which, in turn, results in an excitation-fluence-independent rise time in the TR decay dynamics [30,31]. These consistent results allow us to formulate an assumption about the photocarrier relaxation process in multinary semiconductors, such as CZTSSe and CIGS, in which the band-edge structures are modified strongly by Coulomb interactions between high-density charged defects [30,31].

Whereas the femtosecond TR measurements enable us to investigate the ultrafast energy relaxation of hot carriers after photoexcitation, picosecond THz-TR measurements reveal the recombination dynamics of free carriers in CZTSSe, which plays a particularly important role in the photovoltaic operation of CZTSSe-based solar cells. Figure 4(a) shows the THz-TR kinetic traces of photocarriers in the CZTSSe samples with $x = 0.8$ under different fluences of the 1.52-eV photoexcitation. The THz-TR decay dynamics remains nearly unchanged with increasing excitation fluence. This excitation-fluence-independent behavior of the THz-TR kinetic traces indicates that the single-carrier trapping process dominates the free-carrier dynamics in CZTSSe instead of the two-carrier radiative and the three-carrier Auger recombination [32,33].

Figure 4(b) shows the normalized THz-TR decay dynamics of the photocarriers in CZTSSe samples with different compositions. Interestingly, the THz-TR kinetic traces of the photocarriers in the Se-containing samples ($x = 0$, 0.5, and 0.8) are composed of a single-exponential decay with a time constant ranging from a few picoseconds (for $x = 0$ and 0.5) to several tens of picoseconds (for $x = 0.8$). On the other hand, the THz-TR decay dynamics of the photocarriers in the pure-sulfide samples ($x = 1.0$) are nonexponential and have a nanosecond-scale slow decay component [15,30]. These time constants are consistent with the slow decay times obtained from TR decay dynamics probed near the band-gap energies of CZTSSe, which reveal the lifetimes of photocarriers near the band edge. It can be concluded that the free-carrier lifetime is significantly shortened as the Se content increases.

Considering that a nanosecond-scale decay component was also detected in the nonexponential PL decay dynamics of photocarriers localized to the defects in the CZTS samples ($x = 1.0$) [14,15,20], the slow decay of free carriers in the pure-sulfide samples is due to the thermal excitation of the photocarriers, which are quickly trapped in the high-density shallow band tails after photoexcitation [30,31]. Such a slow nanosecond PL decay was not observed in the Se-containing samples, and this is consistent with the THz-TR decay dynamics, shown in Fig. 4(b). In addition, the free-carrier dynamics in CZTSSe are determined mainly by the single-carrier trapping process. Therefore, it is likely that the fast decay of the free carriers in the Se-containing samples originates from the photocarrier trapping to nonradiative recombination defects. The significant decrease in the free-carrier lifetime with increasing Se concentration manifests a considerable increase in the nonradiative defect concentration. As shown in Fig. 1, a noticeable PL signal is still observed clearly even under a below-band-gap excitation, in which the photocarriers are generated at the spatially localized tail states. Most nonradiative defects in CZTSSe, therefore, are probably deep defects in the forbidden gap. These defects are not likely to be ionized due to thermal activation at room temperature. Consequently, charged defects, which determine primarily the average depth of the electrostatic potential fluctuations γ in CZTSSe [19,22], are mainly due to the shallow defects located near the band edge. In disordered materials where band-gap
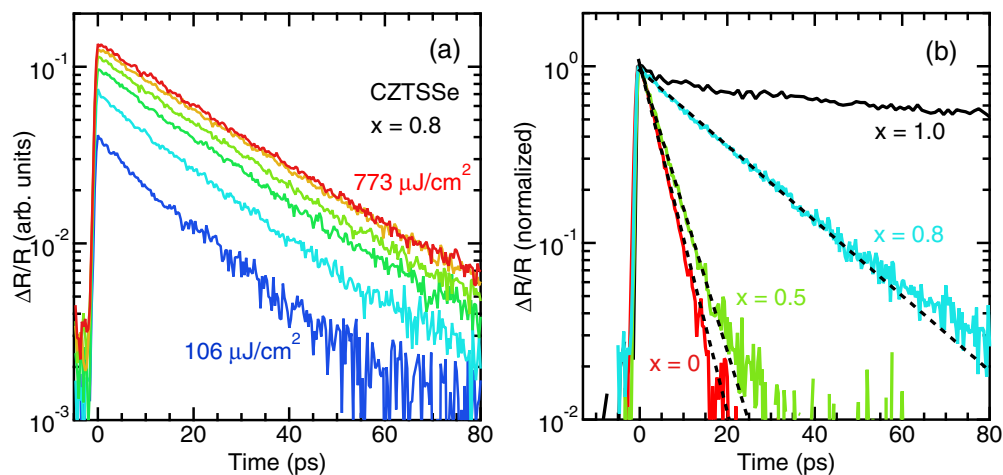

FIG. 4. (Color online) (a) THz-TR decay dynamics ($\Delta R/R$) of the photocarriers in CZTSSe samples with $x = 0.8$ measured under different fluences of the 1.52-eV photoexcitation. (b) Normalized THz-TR decay dynamics of the photocarriers in CZTSSe ($\Delta R/R$) with different S compositions [$x = 0$ (red), 0.5 (green), 0.8 (blue), and 1.0 (black)]. The dashed lines are single-exponential fitting curves.

fluctuations occur due to structural defects and spatially varying alloy composition, band edges of the conduction band and the valence band have inverse spatial fluctuations. The photogenerated electrons and holes, therefore, are not spatially separated, and the carrier lifetime depends inversely on the density of band tails, i.e., a large value of γ causes a fast decay and vice versa [19]. However, in the case of CZTSSe where electrostatic potential fluctuations exist [18–21], electrons and holes are spatially separated; carriers recombine radiatively only through slow tunneling. Thus, it is believed that the carrier lifetime is dominated by tunneling of carriers through barriers and is not related with the value of γ.

So far, we have observed a trade-off between the composition-dependent steady-state and transient optical responses in CZTSSe. Based on the steady-state PL and PLE measurements, we determined that the density and average potential amplitude of band tails existing in CZTSSe are decreased as the Se content increases; this leads to an advantage in using Se-rich CZTSSe absorbers for solar-cell applications [5–7,29]. However, the ultrafast time-resolved measurements established that the energy relaxation of hot carriers and the lifetime of photocarriers in CZTSSe are shortened drastically with increasing Se concentration. Such characteristics of the photocarriers in the Se-containing absorbers are likely to reduce the open circuit voltage of solar cells [34]. It was reported that the free carriers in CIGS thin films have a long lifetime, up to a few nanoseconds, and the hot carriers experience a slow energy relaxation toward the band edge after photoexcitation [31]. CIGS-based solar cells with a conversion efficiency as high as 15% were fabricated using a CIGS absorber with $E_g \sim 1.18$ eV and $\gamma \sim 35$ meV [19], which are also achievable when using a CZTSSe absorber with a Se-rich composition, according to our results. Thus, we believe that the slow energy relaxation of hot carriers and the long photocarrier lifetime may be critically important to realize high-efficiency CZTSSe-based solar cells. Therefore, in addition to obtaining acceptable values for E_g and γ, care should be taken to optimize the Se concentration to achieve sufficiently slow energy relaxation and long photocarrier lifetime in the CZTSSe absorber.

IV. CONCLUSION

In conclusion, through systematic investigations of composition-dependent optical responses of photocarriers in CZTSSe single crystals using a combination of various types of steady-state and time-resolved optical spectroscopy, we observed that the band tails and the photocarrier lifetime in the CZTSSe absorber determine and limit the photovoltaic performance of CZTSSe-based solar cells in addition to the band-gap energy. Whereas the band tails tend to be less severe with increasing Se content, the photocarrier lifetime is drastically shortened. Our results provide insights into the physics behind the low and composition-dependent PCE of CZTSSe-based solar cells and are therefore helpful for directing further efforts for improving their photovoltaic performance.

[1] M. A. Green, K. Emery, Y. Hishikawa, W. Warta, and E. D. Dunlop, Prog. Photovolt: Res. Appl. **23**, 1 (2015).

[2] D. B. Mitzi, O. Gunawan, T. K. Todorov, K. Wang, and S. Guha, Sol. Energy Mater. Sol. Cells **95**, 1421 (2011).

[3] A. Polizzotti, I. L. Repins, R. Noufi, S.-H. Wei, and D. B. Mitzi, Energy Environ. Sci. **6**, 3171 (2013).

[4] S. Ahn, S. Jung, J. Gwak, A. Cho, K. Shin, K. Yoon, D. Park, H. Cheong, and J. H. Yun, Appl. Phys. Lett. **97**, 021905 (2010).

[5] B. Shin, O. Gunawan, Y. Zhu, N. A. Bojarczuk, S. J. Chey, and S. Guha, Prog. Photovolt: Res. Appl. **21**, 72 (2013).

[6] Y. S. Lee, T. Gershon, O. Gunawan, T. K. Todorov, T. Gokmen, Y. Virgus, and S. Guha, Adv. Energy Mater. **5**, 1401372 (2015).

[7] W. Wang, M. T. Winkler, O. Gunawan, T. Gokmen, T. K. Todorov, Y. Zhu, and D. B. Mitzi, Adv. Energy Mater. **4**, 1301465 (2014).

[8] P. Jackson, D. Hariskos, E. Lotter, S. Paetel, R. Wuerz, R. Menner, W. Wischmann, and M. Powalla, Prog. Photovolt. Res. Appl. **19**, 894 (2011).

[9] Y. Yamada and Y. Kanemitsu, Appl. Phys. Lett. **101**, 133907 (2012).

[10] Y. Yamada, T. Nakamura, M. Endo, A. Wakamiya, and Y. Kanemitsu, Appl. Phys. Express **7**, 032302 (2014).

[11] Y. Yamada, T. Nakamura, M. Endo, A. Wakamiya, and Y. Kanemitsu, J. Am. Chem. Soc. **136**, 11610 (2014).

[12] A. Nagaoka, R. Katsube, S. Nakatsuka, K. Yoshino, T. Taniyama, H. Miyake, K. Kakimoto, M. A. Scarpulla, Y. Nose, J. Crystal Growth **423**, 9 (2015).

[13] H. J. Hovel, *Semiconductors and Semimetals, Vol. 11, Solar cells* (Academic, New York, USA,1985).

[14] L. Q. Phuong, M. Okano, Y. Yamada, A. Nagaoka, K. Yoshino, and Y. Kanemitsu, Appl. Phys. Lett. **103**, 191902 (2013).

[15] L. Q. Phuong, M. Okano, G. Yamashita, M. Nagai, M. Ashida, A. Nagaoka, K. Yoshino, and Y. Kanemitsu, Appl. Phys. Express **8**, 062303 (2015).

[16] S. Chen, A. Walsh, X.-G. Gong, and S.-H. Wei, Adv. Mater. **25**, 1522 (2013).

[17] A. P. Levanyuk and V. V. Osipov, Soviet Phys. Usp. **24**, 187 (1981).

[18] M. J. Romero, H. Du, G. Teeter, Y. Yan, and M. M. Al-Jassim, Phys. Rev. B **84**, 165324 (2011).

[19] T. Gokmen, O. Gunawan, T. K. Todorov, and D. B. Mitzi, Appl. Phys. Lett. **103**, 103506 (2013).

[20] L. Q. Phuong, M. Okano, Y. Yamada, A. Nagaoka, K. Yoshino, and Y. Kanemitsu, Appl. Phys. Lett. **104**, 081907 (2014).

[21] J. P. Teixeira, R. A. Sousa, M. G. Sousa, A. F. da Cunha, P. A. Fernandes, P. M. P. Salome, and J. P. Leitao, Phys. Rev. B **90**, 235202 (2014).

[22] B. I. Shklovskii and A. L. Efros, *Electronic Properties of Doped Semiconductors* (Springer Verlag, Berlin, Germany,1979).

[23] J. K. Katahara and H. W. Hillhouse, J. Appl. Phys. **116**, 173504 (2014).

[24] R. Haight, A. Barkhouse, O. Gunawan, B. Shin, M. Copel, M. Hopstaken, and D. B. Mitzi, Appl. Phys. Lett. **98**, 253502 (2011).

[25] C. Persson, J. Appl. Phys. **107**, 053710 (2010).

[26] S. Chen, A. Walsh, J.-H. Yang, X. G. Gong, L. Sun, P.-X. Yang, J.-H. Chu, and S.-H. Wei, Phys. Rev. B **83**, 125201 (2011).

[27] M. Grossberg, J. Krustok, J. Raudoja, K. Timmo, M. Altosaar, and T. Raadik, Thin Solid Films **519**, 7403 (2011).

[28] J. Singh and K. K. Bajaj, Appl. Phys. Lett. **44**, 1075 (1984).

[29] U. Rau and J. H. Werner, Appl. Phys. Lett. **84**, 3735 (2004).

[30] L. Q. Phuong, M. Okano, Y. Yamada, G. Yamashita, T. Morimoto, M. Nagai, M. Ashida, A. Nagaoka, K. Yoshino, and Y. Kanemitsu, Appl. Phys. Lett. **105**, 231902 (2014).

[31] M. Okano, Y. Takabayashi, T. Sakurai, K. Akimoto, H. Shibata, S. Niki, and Y. Kanemitsu, Phys. Rev. B **89**, 195203 (2014).

[32] H. Yasuda and Y. Kanemitsu, Phys. Rev. B **77**, 193202 (2008).

[33] Y. Yamada, H. Yasuda, T. Tayagaki, and Y. Kanemitsu, Phys. Rev. Lett. **102**, 247401 (2009).

[34] B. Ohnesorge, R. Weigand, G. Bacher, A. Forchel, W. Riedl, and F. H. Karg, Appl. Phys. Lett. **73**, 1224 (1998).